Nat. Hazards Earth Syst. Sci. Discuss., 3, 5155–5189, 2015
www.nat-hazards-earth-syst-sci-discuss.net/3/5155/2015/
doi:10.5194/nhessd-3-5155-2015

Natural Hazards and Earth System Sciences
Discussions
Open Access

Transport and bottom accumulation of fine river sediments under typhoon conditions and associated submarine landslides: case study of the Peinan River, Taiwan

A. A. Osadchiev[1], K. A. Korotenko[1], P. O. Zavialov[1], W.-S. Chiang[2], and C.-C. Liu[2]

[1]P. P. Shirshov Oceanology Institute, Moscow, Russia
[2]Tainan Hydraulics Laboratory, National Cheng-Kung University, Tainan, Taiwan

Received: 2 July 2015 – Accepted: 5 August 2015 – Published: 31 August 2015

Correspondence to: A. A. Osadchiev (osadchiev@ocean.ru)

Published by Copernicus Publications on behalf of the European Geosciences Union.

Abstract

A combination of a three-dimensional Eulerian ocean circulation model (POM) and a Lagrangian particle-tracking model (STRiPE) is used to study the fate of fine river sediments discharged by the Peinan River at the north-eastern coast of the Taiwan Island. The composite model is verified against in situ measurements and applied to simulate primary sediment deposition under freshet and typhoon discharge conditions of the Peinan River. It is shown that local wind plays the crucial role in sediment transport and settling at the coastal area through its influence on the river plume dynamics and turbulent mixing in the upper layer. Wind forcing conditions generally determine the location of the sediment deposit area, while its final pattern is defined by coastal circulation with respect to coastal geometry and local bathymetry. In the study region river-born sediments are deposited to the sea floor mainly in the shallow shelf areas. A significant portion of discharged fine sediments is moved offshore to the deeper ocean where it is spread and dissipated by the strong coastal circulation governed by the Kuroshio Current.

The performed numerical experiments showed that sediment accumulation rate under typhoon conditions is about two orders greater comparing to freshet condition. The simulation results were used to identify potential zones of formation of submarine landslides caused by elevated sediment deposition at the steep sea floor during and shortly after the typhoon events. Basing on these results we detected the areas of the continental shelf and continental slope which have high risk of being incised and eroded by autosuspending sediment gravity flows.

1 Introduction

Small rivers transport significant volume of terrigenous sediment to the ocean in the global scale (Milliman and Syvitski, 1992) and affect short-term and long-term coastal and seabed characteristics (Syvitski and Saito, 2007; Milliman et al.,

NHESSD
3, 5155–5189, 2015

2007). Particularly, elevated sediment deposit can initiate submarine landslides and subsequent autosuspending turbidity flows which are abundant at certain coastal areas (e.g., Hampton et al., 1996; Lamb and Mohrig, 2009; Carter et al., 2012; Warrick, 2014). One good example are small mountainous rivers of the Taiwan Island delivering 180–380 million tonnes of terrigenous constituents annually. This relatively large discharge is caused by certain climatic, topographic, lithological, and anthropogenic features of the Taiwan Island (Dadson et al., 2003; Kao et al., 2005; Kao and Milliman, 2008).

The majority of riverine water and sediment are discharged from the Taiwan Island during the monsoon season (June–September) when river and sediment runoff are several orders of magnitude greater comparing with the dry season (Warrick and Milliman, 2003; Mirabito et al., 2012). Even more dramatic intensification of discharge is observed during short-term typhoon events which were registered 255 times during 1949–2009 (Chang et al., 1993; Liu et al., 2006, 2013). On average 60–80 % of sediment load is deposited at the steep eastern and south-western shelves of the island (Liu et al., 2008) which are characterized by elevated seismic activity. Coaction of rapid accumulation and underconsolidation of sediments with earthquake events which are potential triggers of submarine landslides attracts strong research interest to the considered region (e.g., Hsu et al., 2008; Huh et al., 2009; Hale et al., 2012; Carter et al., 2012).

Energetic turbidity flows can erode and transport huge amount of terrigenous material from shelf areas to the deep sea via submarine canyons (Meiburg and Kneller, 2010; Walsh and Nittrouer, 2009). Taiwan rivers are characterised by high concentrations of total particulate organic carbon (Kao and Liu, 1996; Hilton et al., 2008) therefore turbidity currents at the Taiwan shelf play an important role in burial of organic carbon. Also they cause significant number of destruction events of underwater pipelines, telecommunication cables, and other artificial structures at continental shelf and continental slope (Carter et al., 2014). In particular, a number of cable breaks at the eastern and south-western coastal areas of Taiwan Island happened after a Pingtung Earthquake in 2006 caused serious failures in data

NHESSD
3, 5155–5189, 2015

transmission for the whole Asian Pacific region (Hsu et al., 2008). Therefore identification of coastal areas which can be potentially influenced by gravity flows has great practical importance.

Turbidity currents at the Taiwan shelf are mainly caused by two different mechanisms, namely, hyperpycnal river discharge and excrescent accumulation of fine sediment resulting in submarine landslide. The first mechanism, which emergences at river estuaries during typhoon events when river sediment concentration exceeds certain value, was considered in many works (e.g., Dadson et al., 2005; Milliman and Kao, 2005; Milliman et al., 2007). However, much less attention was paid to the second mechanism which also can be induced by elevated sediment runoff during and shortly after typhoon events. It has significantly longer preconditioning period and is characterized by distributed potential sources and potential pathways of turbidity flows (Carter et al., 2014).

This work is focused on investigation of the fate of fine sediment discharged by the Peinan River at the north-eastern coast of the Taiwan Island and related identification of areas of potential formation of submarine landslides based on mass distribution of sediment deposit at the seafloor. Previous studies of river-born sediment dispersal in the coastal areas demonstrated its high variability caused by influence of external forcing factors, namely, volume of sediment discharge, sediment concentration in river water, grain-size distribution, coastal flows including tidal circulation, wave forcing and margin geometry (e.g., Orton and Reading, 1993; Walsh and Nittrouer, 2009). Transport of sediments is determined by motion of a buoyant river plume and ambient coastal circulation which have substantially different dynamic characteristics. As a result many general aspects of sediment delivery at the coastal area remains unclear (Milliman and Kao, 2006; Yu, 2006), which necessitates the specific research of sediment fate at the study area adjacent to the Peinan River estuary.

In this work we use a composite of Lagrangian and Eulerian modelling to reproduce transport and sedimentation of fine terrigenous particles discharged from the Peinan River. For this purpose we track these particles as passive tracers of river outflow using a newly developed Lagrangian model of a Surface-Trapped River Plume Evolution (STRiPE) model within the Peinan river plume. After a particle sinks beneath the plume its movement is governed by coastal circulation simulated by the Princeton Ocean Model (POM). The combination of the models was applied for the study region and validated against in situ measurements. After that we performed numerical experiments to compare the fate of fine sediment under freshet and typhoon forcing conditions and composed relevant maps of mass distribution of sediment deposit at the seafloor. Finally, basing on the modelling results and high-resolution bathymetry we evaluated probability of formation of typhoon-induced submarine landslides at the study area.

The article is organized as follows. Section 2 provides detailed information about the study region and in situ data collected during the field work at the study region in April 2014 and used for the model validation. Section 3 is focused on the general description and implementation of the model. The results of numerical simulations of sediment transport under freshet and typhoon forcing conditions are described in Sect. 4. Discussion of model results and identification of zones of potential submarine landslides at the study area is given in Sect. 5, followed by the summary and the conclusions in Sect. 6.

2 Study area

The study region is located at the south-eastern coast of the Taiwan Island, in the area adjacent to the Peinan River estuary (Fig. 1). The oceanographic conditions off the eastern coast of Taiwan are mainly governed by the Kuroshio Current, tides, winds, and river discharge.

2.1 The Kuroshio Current

The Kuroshio Current (KC) originates from the northern branch of the North Equatorial Current (NEC). After bifurcating of NEC near the Philippine archipelago KC passes

NHESSD
3, 5155–5189, 2015

through the Luzon Strait and flows northward along the eastern coast of the Taiwan Island. On average KC spans from the eastern coast of Taiwan to 100–150 km offshore and its depth reaches down to 800–1000 m (Liang et al., 2003; Hsin et al., 2008). According to in situ data collected by multiple hydrographic surveys and current meter observations the northward transport of KC along the eastern coast of Taiwan is estimated to be about 30 Sv (Hsin et al., 2008). However KC has strong variability ranging from synoptic to inter-annual, in particular at the annual scale it strengthens in summer and weakens in winter (Gilson and Roemmich, 2002). However, the position of KC along the coast changes nonuniformly, particularly in winter it moves significantly offshore the southeastern coast of Taiwan.

The mean Kuroshio Central Position (KCP) is located at about 122.1° E southeast of Taiwan and at about 122.9° E northeast of Taiwan, generally following the eastern coastline (Fig. 1). The largest variability of KCP occurs in the area south of 23° N (Hsin et al., 2013), i.e., within the study region of the current work. The climatology of velocity of KC obtained from in situ measurements is rather complex indicating a multicore structure and several branches of KC located to the east of Taiwan (Yuan et al., 1998; Rudnick et al., 2011).

As KC sweeps off the southern tip of Taiwan, the main stream passes through the gap between the Taiwan Island and the Green Island. The speed of KC at this region is about 1.0 $m s^{-1}$ at the top layer ($0 \sim 200$ m), 0.5 $m s^{-1}$ at the middle layer ($200 \sim 400$ m), and 0.3 $m s^{-1}$ at the bottom layer ($400 \sim 700$ m) respectively according to the field measurements (Shen, 2012). The influence of KC is registered till the depth of 800 m, while water below 800 m is basically motionless.

The small Green Island (about 5 km in diameter) is located at the study region within the energetic mainstream of the KC. It acts as an obstacle in the stream and induces vortexes shedding downstream from the island which can be identified at satellite imagery (Liang et al., 2013). A recirculation wake followed by a wavy tail in the lee of the island observed by satellite imagery (Jia and Liu, 2004) and field measurement (Shen, 2012) causes upwelling and enhances nitrate concentration in the upper ocean.

NHESSD
3, 5155–5189, 2015

This wake covers an area of about 1–2 times greater than the Green Island and is characterized by weak surface current speeds ranging from 0.2 to 0.5 $m s^{-1}$ (Chang et al., 2013).

2.2 Tides

In addition to KC, tides play a great role in coastal circulation at the study area. Tidal circulation at this region is mainly governed by four constituents, namely, two semi-diurnal principal solar tides M2 and S2 with periods 12.42 and 12.00 h respectively, diurnal luni-solar K1, and diurnal lunar O1 with periods 23.93 and 25.82 h respectively (Wyrtky, 1961). A combination of these four components can be used for general description of tidal circulation at the study region.

The tidal range is small and tidal currents are weak (Hu et al., 2010; Zu et al., 2008) along the southeastern coast of Taiwan. Tidal sea level harmonic constants (amplitude in cm φ^{-1}, phase in degrees) for O1, K1, M2, and S2 were found to be equal to 14.75/79.2, 17.54/101.5, 20.6/324.8 and 3.02/67.7 respectively at the tide-gauge station CG (Hu et al., 2010) located in the study region.

2.3 River discharge

Although principal rivers of the Taiwan Island inflow into the Taiwan Strait from the flat western coast, several mountainous rivers of the steeply sloped east coast discharge into the ocean nearly the same amount of suspended sediment (about 150 Mt $year^{-1}$) as those of the west coast (130–220 Mt $year^{-1}$) (Liu et al., 2008). The Peinan River is one of the biggest and the most important rivers of the east coast. Despite its modest length (85 km), basin area (1600 km^2) and moderate mean annual freshwater runoff varying from 30 $m^3 s^{-1}$ in spring to 170 $m^3 s^{-1}$ in summer, the Peinan River discharges a significant volume of sediments equal to 20–90 Mt $year^{-1}$ (Liu et al., 2008; Mirabito et al., 2012). However, river discharge and sediment runoff rates sharply increase during short-term typhoon events abundant for this area. For example, discharge of

NHESSD
3, 5155–5189, 2015

the Peinan River exceeded 6000 $m^3 s^{-1}$ on 9 August 2009 during typhoon Morakot (Mirabito et al., 2012). The sediment concentration in Peinan water is particularly high following intense precipitation events and can exceed 10 $g L^{-1}$ (Dadson et al., 2005; Milliman and Kao, 2005).

2.4 Bathymetry

The steep eastern continental slope of the Taiwan Island is crossed by numerous small submarine canyons, some of them connect river estuaries with deep sea (Ramsey et al., 2009). Bathymetry of the study region is also very complex and irregular as shown in Fig. 2. Its main features away the shoreline are, firstly, the wavy deepening topography with two canyons separated by underwater ridges and Green Island located at 22°50′ N and 121°80′ E, 40 km off the south-eastern coast of Taiwan, and, secondly, the abrupt continental slope which descends from 1000 to 4000 m at the eastern flank of the region (Fig. 1).

Both canyons are stretched in meridional direction and merge into the large Taitung Canyon through which a large volume of sediments derived from the Taiwan mountain belt is transported including heavy sediments and pollutants incoming with the Peinan River waters (Sibuet et al., 2004).

3 In situ data

Field survey within the study area was conducted on 15–17 April 2014 using two local fishery boats. Everyday measurements included continuous registration of temperature and salinity in the upper layer along the ship track at the coastal area influenced by the Peinan buoyant plume using a pump-through CTD system equipped with YSI-6600V2 and YSI EXO-2 instruments. Also vertical CTD profiling from surface to 25 m depth (or to the seabed at shallower stations) and water sampling were performed at the 14 stations situated as shown at Fig. 3.

NHESSD
3, 5155–5189, 2015

A portable meteorological station, continuously recording principal meteorological parameters (wind speed and direction, atmospheric pressure, air temperature and humidity) as 10 min averages, was mounted about 10 m above the sea level at the top of an old lighthouse in the Fugang Fishery Harbor 2.5 km north of the Peinan River estuary.

The obtained data sets were used for validation of the numerical model reproducing dynamics of the Peinan River plume. The detailed description of model validation and comparison of simulation results with the in situ measurements are given in Sect. 5.1.

The form, deposition and spatial extent of the Peinan river plume showed significant variability during the field survey (Fig. 4). On 15–16 April 2014, the freshwater plume (which salinity is lower than 33 psu) was well-developed and stretched along the shore in southwestern direction from the river mouth. Its alongshore propagation and cross-shore width were about 16 and 3 km correspondingly. The inner part of the plume formed a salinity front (25–30 psu) near the river estuary. On the next day of 17 April 2014, the observed plume was arrested near the estuary and propagated slightly in the north-eastern direction. The plume area decreased to quarter of its previous size, however, salinity of the inner part of the plume also significantly reduced and was less than 10 psu. The observed variability of the Peinan river plume was apparently connected with intensification of wind forcing which happened on 16 April. The increase of wind stress from less than 0.005 to about 0.02 $\mathrm{N\,m^{-2}}$ resulted in amplification of plume dissipation as well as caused development of strong offshore currents and subsequent coastal upwellings.

4 Model

As it was mentioned in Sect. 1 transport of fine sediment discharged from river has two different phases governed by dynamics of buoyant river plume and ambient coastal circulation. This fact is the reason for joint usage of two numerical models organized in a nested configuration which complement each other in simulating complex sediment transport process. An outer model is a well-known finite difference σ-coordinate Princeton Ocean Model (POM) which reproduces general ocean circulation along the north-eastern coast of Taiwan with 1 nautical minute spatial resolution. It provides boundary conditions for the inner Surface-Trapped River Plume Evolution model (STRiPE) which is focused on high-resolution simulation of dynamics of a buoyant river plume. Transport and settling of fine sediment within the nested model is simulated using combination of deterministic approach representing tracking of a passive tracer (James, 2002) and stochastic random-walk scheme parametrizing spatially non-uniform turbulent mixing (Ross and Sharples, 2004). The detailed description of model configuration and its implementation is given below.

4.1 POM module

The POM module consists of a 3-D primitive equation ocean model with level 2.5 Mellor–Yamada turbulence closure scheme (Blumberg and Mellor, 1987; Mellor and Yamada, 1982) and complete thermodynamics implemented. The model domain covers the area from 120.9 to 122.0° E and from 22.3 to 23.5° N (Fig. 2) and has three open boundaries at the northern, western and southern borders of the region. It is divided into 68 × 75 grid cells with a size of one nautical minute in both longitudinal and latitudinal directions, i.e., the average zonal and meridional resolutions are equal to 1.723 km (at 23° N) and 1.836 km correspondingly. The vertical sigma coordinate is represented by 31 levels with irregular distribution. They cover the water column from 5 to 4860 m which is stretched at upper and bottom levels for realistic reproducing of surface and bottom boundary layers. The time steps were set equal to 3 and 120 s for the external and internal modes correspondingly.

The vertical eddy viscosity and diffusivity were provided by the Mellor–Yamada turbulence closure scheme with a background value of $10^{-5}\,m^2\,s^{-1}$. The horizontal

NHESSD
3, 5155–5189, 2015

eddy viscosity K_L was calculated using the embedded Smagorinsky formula

$$K_\mathrm{L} = C_\mathrm{H} \Delta x \Delta y \sqrt{\left(\frac{\partial U}{\partial x}\right)^2 + \left(\frac{\partial V}{\partial y}\right)^2 + \frac{1}{2}\left(\frac{\partial U}{\partial y} + \frac{\partial V}{\partial x}\right)^2}, \quad (1)$$

where U and V are the horizontal components of mean velocity, C_H is a scaling parameter equal to 0.1. Horizontal eddy diffusivity was obtained using the inverse Prandtl number of 0.5.

As was mentioned above, the submarine canyons and ridges stretching along the shore are the important features of the bottom topography. They may significantly affect the structure of the alongshore flow and mixing governed by the interacting tidal circulation and KC. Therefore it is important to adequately simulate bottom stress in order to represent these effects.

In the POM module bottom friction is determined by current velocity of the layer closest to the seabed using the assumption of a logarithmic current profile in the following way. The stress components τ_b^x and τ_b^y induced by the bottom friction are described as

$$\left(\frac{\tau_\mathrm{b}^x}{\rho}, \frac{\tau_\mathrm{b}^y}{\rho}\right) = C_z \left(U^2 + V^2\right)^{1/2} (U, V), \quad (2)$$

where C_z is a non-dimensional coefficient depending on the roughness length of the bed z_0 and the water depth H

$$C_z = \max\left(\frac{\kappa^2}{\left\{\ln\left[\left(1 + \sigma_{kb-1}\right) H/z_0\right)\right]\right\}^2}, 0.0025\right), \quad (3)$$

where κ is the von Karman constant equal to 0.4, $\sigma_{\mathrm{kb-1}}$ is the depth of the layer overlying the sea bottom in sigma coordinates.

Temperature and salinity boundary conditions applied at the open boundaries of the calculation domain were different for inflow and outflow fluxes (Fig. 2). Temperature T and salinity S of inflow water were set equal to the corresponding open boundary values, while in the case of outflow from the domain the radiation equation was used:

$$\frac{\partial}{\partial t}(T,S) + U_n \frac{\partial}{\partial n}(T,S) = 0, \tag{4}$$

where n represents the direction normal to the open boundary. The radiation boundary conditions are based on the principle of propagation of a long gravity wave which is used to specify sea level oscillations in the form of a combination of values of level elevations and a normal current velocity component at the open boundaries.

The vertically averaged barotropic velocities at the open boundaries of the model domain were estimated using the Flather (1976) formula:

$$\overline{U}_\mathrm{n} = \overline{U}_\mathrm{n}^0 + \sqrt{\frac{g}{H}}(\eta - \eta_0) \tag{5}$$

where $\overline{U}_\mathrm{n}$ is the vertically averaged normal component of the velocity at the open boundary at time t, $\overline{U}_\mathrm{n}^0$ is the initial vertically averaged normal component, η is the model sea surface elevation calculated using the continuity equation and located half of a grid inside of the open boundary in the model domain, η_0 is the sea surface elevation at the open boundary of the model, H is the water depth on the open boundary, and g is gravitational acceleration. Open boundary conditions $\overline{U}_\mathrm{n}^0$ and η_0 were implemented from the THL barotropic tidal model (Hu et al., 2010) kindly provided by Liu et al. (2014).

4.2 STRiPE module

STRiPE is a Lagrangian model developed for simulating river plumes under various forcing conditions. It represents a river plume as a set of Lagrangian “particles” or homogeneous elementary water columns extending from the surface down to the

NHESSD
3, 5155–5189, 2015

boundary between the plume and the underlying sea water. These particles are released from the river mouth with the initial velocity depending on discharge rate. Then they are tracked by the model according to the momentum equations reproducing the main forces that determine river plume dynamics, namely, the Coriolis force, the force applied from the wind, the friction with the underlayer flow, the lateral friction, the pressure gradient force, and small-scale horizontal turbulent mixing parameterized by the random-walk method. The background velocity field which is necessary for calculating bottom friction is incorporated from POM simulations as input data. At every step of the model integration, the overall set of particles represents the river plume, and hence the temporal evolution of the plume structure is obtained. Horizontal turbulent diffusivity K_h used in the random-walk scheme is parameterized by the Smagorinsky diffusion formula described in Sect. 3.1. Vertical mixing of particles with the ambient seawater is parametrized by the salinity diffusion equation:

$$\frac{\partial S}{\partial t} = K_v \frac{\partial^2 S}{\partial z^2}, \tag{6}$$

where S is the particle salinity, and K_v is the vertical diffusion coefficient parameterized via the Richardson number Ri and scaling coefficient C_v as given in Large (1994):

$$D_v = C_v \left(1 - \min\left(1, vRi^2\right)\right)^3. \tag{7}$$

The detailed description of the STRiPE is given in Osadchiev and Zavialov (2013). This model coupled with POM was recently used to study dynamical features of the Zhuoshui and Wu river plumes located at the western part of Taiwan coast (Korotenko et al., 2014).

4.3 Sediment transport module

Transport and settling of fine suspended sediments discharged from the river mouth is simulated using a Lagrangian particle-tracking module. Both horizontal and vertical

NHESSD
3, 5155–5189, 2015

movements of a sediment particle are calculated using a combination of a deterministic component defined by motion of ambient water and sinking of a particle under the gravity force and a stochastic random-walk scheme that reproduces influence of small-scale turbulent mixing. Particles are initially released from the river mouth and their horizontal transport is determined by internal dynamics of a river plume simulated by the STRiPE module. We presume strong mixing in river water before it inflows into the sea, therefore particles have homogenous vertical distribution in the inflowing water. Initial concentration of particles in river water was evaluated according to the following equation (Nash, 1994):

$$C = aQ^b \tag{8}$$

where C is the sediment concentration in river water, Q is the river discharge volume, a and b are the scaling coefficients.

During its motion a particle sinks within the river plume till it reaches the mixing zone between the river plume and underlying sea waters. After a particle descends beneath the lower plume boundary its motion is determined by ambient coastal circulation calculated by the POM module. In this study we focus on relatively small particles with diameter less than 10^{-4} m, therefore gravity induced vertical motion is determined by a Stokes' law, and particle settling velocity w_s is calculated according the well-known formula (Stokes, 1851):

$$w_s = \frac{gd^2(\rho_s - \rho_w)}{18\mu\rho_w}, \tag{9}$$

where g is the gravitational acceleration, d is the diameter of a sediment particle, ρ_s is the density of a sediment particle, ρ_w is the density of water, μ is the dynamic water viscosity.

Total vertical particle displacement caused by sinking under gravity force, vertical circulation of ambient water, and turbulent mixing was parametrized using the following

NHESSD
3, 5155–5189, 2015

equation (Hunter et al., 1993; Visser, 1997; Ross and Sharples, 2004) which represents features of spatially non-uniform turbulent mixing:

$$\Delta z = \left(w_S + \frac{\partial K}{\partial z} \right) \Delta t + \sqrt{\frac{2}{3} K_v \left(z + \frac{1}{2} \frac{\partial K_v}{\partial z} \Delta t \right) \Delta t} \xi, \quad (10)$$

where Δz is the vertical particle displacement, w_s is the Stokes' settling velocity of a particle, K_v is the vertical eddy diffusivity coefficient, Δt is the time step, ξ is a random process with standard normal distribution (zero mean and unity variance) produced by a random number generator.

The sediment transport module domain covers the area from 120.9 to 121.4° E and from 22.5 to 22.9° N and has realistic shoreline. The domain topography was set with a step equal to 0.002° for both latitude and longitude directions with 1 m accuracy.

The described model was applied to simulate transport of sediments discharged by the Peinan River under several important simplifications. Firstly, we presume particles as having spherical shape and do not consider flocculation and deflocculation processes, which can dramatically change settling velocity and thus sediment transport pathways and deposition patterns (e.g., Sholkovitz, 1975; Droppo and Ongley, 1994). However, simulation of flocculation/deflocculation and settling of non-spherical particles is worthwhile only in conjunction with precise input data of sediment concentration in river water and grain size distribution. These data sets are generally not available especially for considered typhoon conditions due to complexity of the related in situ measurements. Therefore we use only approximate values of these data basing on previous studies of river sediments under freshet and typhoon conditions.

Secondly, the transport module simulates only primary deposition of particles and does not consider subsequent bottom sediment resuspension. However in this study we focus on of sediment transport in relatively short time scales, therefore secondary sediment redistribution caused by resuspension processes does not result in large displacement of sediments comparing to primary transport especially during and shortly after typhoon events. As a result resuspension does not significantly modify the primary sediment deposition patterns obtained by the model.

5 Numerical simulations

The developed model was applied to the study region to investigate fate of fine sediments discharged by the Peinan River. The POM module was initialized using the Antonov et al. (2010) seasonally averaged climatic temperature and salinity fields as the initial background conditions and provided the ambient velocity fields for the STRiPE and sediment transport modules.

At the STRiPE module freshwater particles containing sediment constituents were released from the Peinan River estuary according to the Manning formula with the initial inflow velocity $w = 0.3(\frac{Q}{L})^{2/5}$, where Q is the discharge of the Peinan River, L is the width of the Peinan River mouth. The initial vertical scale of the released freshwater columns (i.e. the plume thickness at the mouth) was prescribed as $h = 3.3(\frac{Q}{L})^{3/5}$. Initial sediment concentration in the inflowing river waters was calculated according to Eq. (8), the coefficients $a = 0.25$ and $b = 0.6$ for $Q < 500\,\mathrm{m^3\,s^{-1}}$ and $a = 0.02$ and $b = 1.0$ for $Q > 500\,\mathrm{m^3\,s^{-1}}$ specifying the dependence between river discharge and sediment concentration for the Peinan River under typhoon conditions were taken from Milliman and Kao (2005). Densities of river and ambient sea waters were equal to 1000 and 1033 $\mathrm{kg\,m^{-3}}$ correspondingly, while sediment density was prescribed as 1300 $\mathrm{kg\,m^{-3}}$. Initial grain distribution of fine sediments was prescribed according to the results of analysis of the water samples taken at the 1 m depth at the station situated 50 m offshore from the Peinan River mouth (Fig. 3). Kinematic viscosity of water was set equal to $10^{-6}\,\mathrm{m^2\,s^{-1}}$. The integration time steps for the STRiPE and sediment transport modules were set to 10 min.

The numerical experiments were organized in the following way. Firstly, we validated the model against the in situ data collected during the field survey. Then we simulated the behaviour of the Peinan river plume and the associated transport of fine sediments under average summer freshet and typhoon conditions.

5.1 Validation

The first simulation was performed under wind forcing and Peinan discharge rate observed during the field work at the meteorological station located at the Peinan estuary and gauge station located at the Taitung Bridge correspondingly. The period of 15–17 April 2014 was dominated by the south-western wind, its magnitude ranged from 0.5 to 6 $\mathrm{m\,s^{-1}}$. Peinan River had stable discharge equal to 21 $\mathrm{m^3\,s^{-1}}$.

The behaviour of the Peinan river plume during 15–17 April 2014 was simulated by the STRiPE module using in situ wind and discharge data and POM-generated current velocity field. The numerical modelling adequately reproduced synoptic variability of the Peinan River plume observed during the field survey. The Peinan plume was stretched along the shore in south-western direction on 15–16 April, however upwelling-favourable south-western winds resulted in shift of the plume to the north of the Peinan estuary and widening of the plume on 17 April. The average positions of the simulated plume corresponding to 16 and 17 April 2014 illustrate this dramatic displacement and show good agreement with the salinity maps of the region obtained from the CTD measurements (Fig. 4). As a result the validation experiment proved good ability of the developed model to reproduce dynamics of the Peinan river plume.

5.2 Numerical experiments

After validation of the model, we performed two numerical experiments reproducing fate of river-born sediments under moderate and flooding discharge conditions of the Peinan River. The first simulation of sediment transport under moderate discharge conditions was excecuted using average August discharge of the Peinan River (80 $\mathrm{m^3\,s^{-1}}$) and average climatic wind conditions (NE wind, 2.0 $\mathrm{m\,s^{-1}}$). The first experiment was performed for the period of 30 days.

NHESSD
3, 5155–5189, 2015

Model configuration for the second numerical experiment reproducing sediment transport under flooding discharge conditions was more complex. Initially, the plume was modelled under average August climatic conditions for a period of three days. After that, we simulated six days of flooding conditions using wind forcing and discharge rate of the Peinan River observed on 4–9 August 2009, when typhoon Morakot was passing over Taiwan. Next, during the relaxation period the model was forced again by mean climatic conditions for August. Typhoon Morakot induced rainfall over the eastern coast of Taiwan and led to an unprecedented rainfall and subsequent flooding in the southern Taiwan (Wu et al., 2011). Discharge rate of the Peinan River peaked from the annual mean of 80–6000 $m^3 s^{-1}$, while a maximal intensity of wind exceeded 40 $m s^{-1}$ (Mirabito et al., 2012).

The hydrodynamical model shows a significant impact of typhoon conditions on the sea circulation east of Taiwan and behavior of the Peinan plume. Strengthening of south-westerly winds over the study area and increase of the Peinan River discharge induced by the typhoon resulted in tremendous change of local circulation and considerable elongation of the Peinan plume (Fig. 5). Initially, the bulge-like river plume was stretched northwardly along the shore under the action of average climatic winds (Fig. 5a). The interaction of wind drift current and buoyancy resulted in the strong jet-like alongshore current north of the Peinan estuary.

Increase of wind stress and change of its direction during the first day of the typhoon caused plume to widen, to shift in southern direction and to detach from the shore (Fig. 5b). During the second typhoon day the plume moved in the northeastern direction, its newly formed part adjacent to the Peinan estuary propagated along the coast, while the older part formed a round-shape bulge which extension reached the Green Island (Fig. 5c). The third flooding day was characterized by peaks of wind speed, river discharge, and velocity of coastal circulation (1 $m s^{-1}$). For this day, the plume was stretched north-eastwardly and detached from the coast near 23° N (Fig. 5d). Figure 5e shows the Peinan plume on 10 August 2009 when discharge rate decreased below 2000 $m^3 s^{-1}$, but wind remained strong and its magnitude exceeded

NHESSD
3, 5155–5189, 2015

$10\,m\,s^{-1}$. For this period the meandering plume became unstable in its near-field and was broken into several patches. The far-field of the plume remained solid, but its salinity contrasts with those of ambient water noticeably diminished. After departure of the typhoon from the study area, the north-eastward current was decreasing gradually during several next days. The Peinan plume was tending to return to its position and shape as they were before the typhoon (Fig. 5a).

6 Results and discussion

6.1 Sediment deposition

The obtained simulation results of river-born sediment delivery after 30 days of freshet conditions and 6 days of the typhoon are presented at Fig. 6. Sediment outflow concentration in the Peinan River water was equal to $4\,kg\,m^{-3}$ during the moderate discharge simulation which result in 0.8×10^6 tons of sediment discharge for the period of 30 days. Typhoon conditions were characterized by dramatic increase of river runoff and sediment concentration with the peak values of about $6000\,m^3\,s^{-1}$ and $120\,kg\,m^{-3}$ correspondingly. The total sediment influx during the 6 typhoon days was about 20×10^6 tons which is 25 times greater comparing to the moderate discharge simulation. As a result the sediment accumulation rate under typhoon discharge conditions was about two orders of magnitude greater comparing to average freshet discharge.

The resulting deposit patterns obtained by the two model runs were significantly different. During freshet discharge period river-born sediments were almost homogenously deposited at the shallow area in the southern and south-western directions from the river estuary. The alongshore extent of the area influenced by active sediment load (3–$5\,kg\,m^{-2}$) exceeded 25 km. Total sediment load to the seabed at the study area was about 0.5×10^6 tons, while 0.3×10^6 tons of fine sediments remained in water column and did not settle to the sea floor during the simulation period.

The most active sediment load during and shortly after typhoon period took place within the small area adjacent to the Peinan River estuary. Spatial scale of this area was only 5 km, however its bottom sediment concentration exceeded 300 $kg\,m^{-2}$. A large volume of sediment was also transported form the Peinan river mouth along the shore in the south-western and north-eastern directions and settled to the seabed at the corresponding shallow shelf areas. The spatial extents and bottom sediment concentrations at the considered coastal zones influenced by active sediment loads were equal to 10 km and 150–250 $kg\,m^{-2}$ for the south-western zone and 5 km and 50–150 $kg\,m^{-2}$ for the north-eastern zone. However, only about 8×10^6 tons of the total sediment discharge volume settled at the sea floor within the study area, while 12×10^6 tons were transported offshore to the deeper sea and remained in the water column.

The presented simulation results show that sediment deposition patterns for both model runs significantly depend on the river plume dynamics. Under moderate discharge conditions wind forcing and Coriolis force determine the alongshore spread of the Peinan plume. As a result river-born sediments, which are initially concentrated in the upper layer, are transported by the plume in the south-western direction. Once sediment particles sink beneath the plume their motion is determined by the north-eastward coastal circulation governed by the KC. The average velocity of coastal currents below the upper layer is significantly less than the velocity of the river plume propagation. Therefore sediment particles settled from the plume to the underlying waters at shallow coastal areas located to the south-western from the Peinan estuary are not significantly displaced by coastal currents in the north-eastern direction and are finally deposited to the seabed at this area. On the other hand, a significant portion of sediments at the study region are transported by the plume offshore from the narrow continental shelf. Once these sediment particles sink beneath the plume at deeper ocean, they are moved away in north-eastward direction by the strong alongshore current and do not settle at the sea floor within the study region.

NHESSD
3, 5155–5189, 2015

Elevated discharge of terrigenous sediments to the sea during typhoon conditions resulted in increased sediment deposit at the study area. However, the rate of deposited sediments in respect to the total discharge (40 %) was significantly lower comparing to the freshet conditions (65 %) because of the following reasons. Typhoon conditions are characterized by strong winds which governed spread of the Peinan plume at the study region. During the simulation period the Peinan plume propagated mostly in the north-eastern direction, therefore river-born sediments settled mainly in the small shallow area adjacent to the river plume. Also the plume propagation velocity was significantly higher comparing to the freshet conditions, therefore the majority of the sediments did not sink beneath the plume within this shallow area and were transported offshore to the deeper ocean. Finally, strong wind forcing induced active turbulence at the upper layer, which reduced settling speed of the sediment particles. A short period of northern winds during the typhoon resulted in active sediment deposition at the shallow coastal area situated to the south from the Peinan estuary, however the volume of sediment load at this area was much less comparing to the area adjacent to the Peinan estuary.

6.2 Submarine landslides

One of the practical aims of this study consists in identification of the zones at the study area adjacent to the Peinan River estuary which have high risk of formation of submarine landslides, which can cause autosuspending gravity flows at the steep continental slope. However, in this study we do not focus on triggering processes that cause gravity flows. We study dependences of sediment deposit patterns on external forcing conditions as one of the major preconditioning factor which derives possibility of formation of a submarine landslide and a subsequent turbidity flow. Using the obtained mass distribution of sediment deposit we can calculate downslope component of gravity force applied to the sediment in the following way: $F = m \times \sin(\alpha)$, where m is the mass of sediment deposit to the considered seabed area and α is the slope angle. This value is proportional to the rate of overpressure which cause a submarine landslide

NHESSD
3, 5155–5189, 2015

if exceeds a certain value which depend on local bottom friction. Thus, seabed areas with high values of F situated at the narrow shelf of the study region are the potential regions of formation of autosuspending gravity flows.

We considered distribution of F for typhoon conditions because for this case the average "sliding" force was several orders greater than for sediment distributions formed under moderate discharge conditions. Figure 7 shows relative possibility of formation of submarine landslides (green colour) as well as illustrates paths of the related turbidity flows which will propagate in direction of maximal topography gradient (red colour). As it can be seen, the most possible region of formation of submarine landslides at the study area is located near the Peinan River estuary, which is characterized by the most active sedimentation under typhoon conditions. Pathways of the turbidity flows generated in this zone cover large coastal area situated to the south-east from the Peinan River estuary.

7 Summary and conclusions

This study is focused on influence of external forcing conditions on transport and deposition of fine sediment discharged by the Peinan River plume at the steep north-eastern coast of the Taiwan Island. For this purpose we used a combination of two hydrological numerical models, namely, the Euleruan Princeton Ocean Model (POM) and the Lagrangian Surface-Trapped River Plume Evolution (STRiPE) model. This composite model was validated against in situ measurements performed in the study area on 15–17 April 2014. Then it was used to simulate the fate of river-born sediments discharged during a typical freshet period and during a strong typhoon. For the first numerical experiment we used average climatic August discharge and wind forcing conditions, while the second model run was performed under forcing conditions observed during the Morakot typhoon on 4–9 August 2009.

Numerical experiments showed that initial transport of terrigenous material is mainly governed by river plume dynamics, while its final deposition depends on the local

NHESSD
3, 5155–5189, 2015

coastal circulation of the ambient ocean and the local bathymetry. In particular, the most active sediment deposition at the study region took place at the shallow shelf areas. Sediment particles, which were initially transported by the river plume offshore to the continental slope and deep sea were spread and dissipated by strong coastal circulation governed by the Kuroshio Current before they reached the sea floor.

Strong wind forcing during the typhoon wind increased turbulence at the upper layer and therefore decreased sediment settling speed during its transport by the river plume. On the other hand, elevated wind stress resulted in high velocity of plume propagation, therefore a larger fraction of sediments was transported offshore from the shallow shelf before it sinked beneath the plume. These factors result in a lower ratio of sediment deposit volume to total sediment influx comparing to freshet conditions.

Elevated sediment runoff during typhoon event can result in slope instabilities at the areas of active sediment loads. Therefore basing on the simulation results we detected the zones within the study area which are characterized by high possibility of submarine landslide formation. Also we identified the potential pathways of autosuspending gravity flows induced by the submarine landslides. The obtained results have certain practical implication related to construction of artificial structures such as telecommunication cables and underwater pipelines on the seafloor at the study region.

Acknowledgements. Funding of this research was provided by Russian Scientific Foundation, research project 14-50-00095 (model development and numerical experiments) and Tainan Hydraulics Laboratory, National Cheng-Kung University, Taiwan (field work and data analyses). Authors wish to thank Aleksandr Izhitsky and Aleksandr Grabovsky for valuable support during the fieldwork and many colleagues at THL for their hospitality and assistance.

References

Antonov, J. I., Seidov, D., Boyer, T. P., Locarnini, R. A., Mishonov, A. V., Garcia, H. E., Baranova, O. K., Zweng, M. M., and Johnson, D. R.: World Ocean Atlas 2009, Volume 2: Salinity, edited by: Levitus, S., NOAA Atlas NESDIS 69, U.S. Government Printing Office, Washington, D.C., 184 pp., 2010.

NHESSD

3, 5155–5189, 2015

Transport of river sediments and associated submarine landslides

A. A. Osadchiev et al.

Blumberg, A. F. and Mellor, G. L.: A description of a three-dimensional hydrodynamic model of New York harbor region, J. Hydraul. Eng., 125, 799–816, 1987.
Carter, L., Milliman, J. D., Talling, P. J., Gavey, R., and Wynn, R. B.: Near-synchronous and delayed initiation of long run-out submarine sediment flows from a record-breaking river flood, offshore Taiwan, Geophys. Res. Lett., 39, L12603, doi:10.1029/2012GL051172, 2012.
Carter, L., Gavey, R., Talling, P., and Liu, J.: Insights into submarine geohazards from breaks in subsea telecommunication cables, Oceanography, 27, 58–67, 2014.
Chao, S. Y.: River-forced estuarine plume, J. Phys. Oceanogr., 18, 72–88, 1988.
Chang, C.-P., Yeh, T.-C., and Chen, J. M.: Effects of terrain on the surface structure of typhoons over Taiwan, Mon. Weather Rev., 121, 734–752, 1993.
Chang, M.-H., Tang, T. Y., Ho, C.-R., and Chao, S.-Y.: Kuroshio-induced wake in the lee of Green Island off Taiwan, J. Geophys. Res.-Oceans, 118, 1508–1519, 2013.
Chuang, W.-S.: Dynamics of subtidal flow in Taiwan Strait, Journal of Oceanographic Society of Japan, 41, 65–72, 1985.
Chuang, W.-S.: A note on the driving mechanisms of current in Taiwan Strait, Journal of Oceanographic Society of Japan, 42, 355–361, 1986.
Dadson, S., Hovius, N., Pegg, S., Dade, W. B., Horng, M. J., and Chen, H.: Hyperpycnal river flows from an active mountain belt, J. Geophys. Res., 11, F04016, doi:10.1029/2004JF000244, 2005.
Droppo, I. and Ongley, E.: Flocculation of suspended sediment in rivers of Southeastern Canada, Water Res., 28, 1799–1809, 1994.
Flather, R. A.: A tidal model of the North-West European continental shelf, Memoires de la Societe Royale des Sciences de Liege, 10, 141–164, 1976.
Fong, D. A. and Geyer, W. R.: The alongshore transport of freshwater in a surface trapped river plume, J. Phys. Oceanogr., 32, 957–972, 2002.
Garcia Berdeal, I., Hickey, B. M., and Kawase, M.: Influence of wind stress and ambient flow on a high discharge river plume, J. Geophys. Res., 107, 3130–3151, 2002.
Garvine, R. W.: Estuary plumes and fronts in shelf waters: a layer model, J. Phys. Oceanogr., 17, 1877–1896, 1987.
Geyer, W. R., Hill, P. S., and Kineke, G. C.: The transport, transformation and dispersal of sediment by buoyant coastal flows, Cont. Shelf. Res., 24, 927–949, 2004.
Gilson, J. and Roemmich, D.: Mean and temporal variability of Kuroshio geostrophic transport south of Taiwan (1993–2001), J. Oceanogr., 58, 183–195, 2002.

NHESSD
3, 5155–5189, 2015

Hale, R. P., Nittrouer, C. A., Liu, J. T., Keil, R. G., and Ogston, A. S.: Effects of a major typhoon on sediment accumulation in Fangliao Submarine Canyon, SW Taiwan, Mar. Geol., 326, 116–130, 2012.
Hampton, M. A., Lee, H. J., and Locat, J.: Submarine landslides, Rev. Geophys., 34, 33–59, 1996.
Hilton, R. G., Galy, A., and Hovius, N.: Riverine particulate organic carbon from an active mountain belt: importance of landslides, Global Biogeochem. Cy., 22, GB1017, doi:10.1029/2006GB002905, 2008.
Hsin, Y.-C., Wu, C.-R., and Shaw, P.-T.: Spatial and temporal variations of the Kuroshio east of Taiwan, 1982–2005: a numerical study, J. Geophys. Res., 113, C04002, doi:10.1029/2007JC004485, 2008.
Hsin, Y.-C., Qiu, B., Chiang, T.-L., and Wu, C.-R.: Seasonal to interannual variations in the intensity and central position of the surface Kuroshio east of Taiwan, J. Geophys. Res., 118, 4305–4316, doi:10.1002/jgrc.20323, 2013.
Hsu, S.-K., Kuo, J., Lo, C.-L., Tsai, C.-H., Doo, W.-B., Ku, C.-Y., and Sibuet, J.-C.: Turbidity currents, submarine landslides and the 2006 Pingtung earthquake off SW Taiwan, Terr. Atmos. Ocean Sci., 19, 767–772, 2008, http://www.ocean-sci.net/19/767/2008/.
Hu, C. K., Chiu, C. T., Chen, S. H., Kuo, J. Y., Jan, S., and Tseng, Y. H.: Numerical simulation of barotropic tides around Taiwan, Terr. Atmos. Ocean. Sci., 21, 71–84, 2010.
Huh, C.-A., Lin, H.-L., Lin, S., and Huang, Y.-W.: Modern accumulation rates and a budget of sediment off the Gaoping (Kaoping) River, SW Taiwan: a tidal and flood dominated depositional environment around a submarine canyon, J. Marine Syst., 76, 405–416, 2009.
Hunter, J. R.: Application of Lagrangian particle-tracking technique to modeling of dispersion in the sea, in: Numerical Modelling: Applications for Marine Systems, edited by: Noye, J., North Holland, Amsterdam, 257–269, 1987.
Hunter, J. R., Craig, P. D., and Phillips, H. E.: On the use of random walk models with spatially variable diffusivity, J. Comput. Phys., 106, 366–376, 1993.
James, I. D.: Modelling pollution dispersion, the ecosystem and water quality in coastal waters: a review, Environ. Modell. Softw., 17, 363–385, 2002.
Jan, S., Chern, C.-S., Wang, J.: Transition of tidal waves from the East to South China Sea over Taiwan Strait: influence of the abrupt step in the topography, J. Oceanogr., 58, 837–850, 2002.

Jia, Y. and Liu, Q.: Eddy shedding from the Kuroshio bend at Luzon Strait, J. Oceanogr., 60, 1063–1069, 2004.

Kao, S.-J. and Liu, K.-K.: Particulate organic carbon export from a subtropical mountainous river (Lanyang-His) in Taiwan, Limnol. Oceanogr., 41, 1749–1757, 1996.

Kao, S.-J., Chan, S. C., Kuo, C. H., and Liu, K. K.: Transport-dominated sediment loading in Taiwanese rivers: a case study from the Ma-an Stream, J. Geol., 113, 217–225, 2005.

Kilcher, L. F., Nash, J. D., and Moum, J. N.: The role of turbulence stress divergence in decelerating a river plume, J. Geophys. Res., 117, C05032, doi:10.1029/2011JC007398, 2012.

Korotenko, K. A., Osadchiev, A. A., Zavialov, P. O., Kao, R.-C., and Ding, C.-F.: Effects of bottom topography on dynamics of river discharges in tidal regions: case study of twin plumes in Taiwan Strait, Ocean Sci., 10, 863–879, doi:10.5194/os-10-863-2014, 2014.

Lamb, M. P. and Mohrig, D.: Do hyperpycnal-flow deposits record river-flood dynamics?, Geology, 37, 1067–1070, 2009.

Large, W. G., McWilliams, J. C., and Doney, S. C.: Oceanic vertical mixing: a review and a model with a nonlocal boundary layer parameterization, Rev. Geophys., 32, 363–403, 1994.

Liang, W.-D., Tang, T. Y., Yang, Y. J., Ko, M. T., and Chuang, W.-S.: Upper-ocean currents around Taiwan, Deep-Sea Res. Pt. II, 50, 1085–1105, 2003.

Liu, C.-C., Chiu, Y.-F., Lee, J.-F., Su, C.-H., Chen, M.-T., Lee, C.-T.,Tu, L.-F., and Cheng, P.-C.: Enhancement of Marine Meteorology Simulation Technology on Coastal and Harbor Areas (1/2), Institute of Harbor and Marine Technology Center, Ministry of Transportation and Communication, Taichung City, Taiwan (R.O.C.), ISBN978-986-04-0453-1, 2014.

Liu, J. P., Liu, C. S., Xu, K. H., Milliman, J. D., Chiu, J. K., Kao, S. J., and Li, S. W.: Flux and fate of small mountainous rivers derived sediments into the Taiwan Strait, J. Geol., 256, 65–76, 2008.

Meiburg, E. and Kneller, B.: Turbidity currents and their deposits, Annu. Rev. Fluid Mech., 42, 135–156, 2010.

Mellor, G. L. and Yamada, T.: Development of a turbulent closure model for geophysical fluid problems, Rev. Geophys. Space Ge., 20, 851–875, 1982.

Milliman, J. D. and Kao, S.-J.: Hyperpycnal discharge of fluvial sediment to the ocean: impact of super-typhoon Herb (1996) on Taiwanese rivers, J. Geol., 113, 503–516, 2005.

Milliman, J. D. and Kao, S.-J.: Hyperpycnal discharge of fluvial sediment to the ocean: impact of super-typhoon Herb (1996) on Taiwanese rivers: a discussion, J. Geol., 114, 766–766, 2006.
Milliman, J. D. and Syvitski, J. P. M.: Geomorphic/tectonic control of sediment discharge to the ocean: the importance of small mountainous rivers, J. Geol., 100, 525–544, 1992.
Milliman, J. D., Lin, S. W., Kao, S. J., Liu, J. P., Liu, C. S., Chiu, J. K., Lin, Y. C.: Short-term changes in seafloor character due to flood-derived hyperpycnal discharge: typhoon Mindulle, Taiwan, July 2004, Geology, 35, 779–782, 2007.
Mirabito, C., Haley Jr., P., Lermusiaux, P. F. J., and Leslie, W. G.: A River Discharge Model for Coastal Taiwan during Typhoon Morakot, Rep. MSEAS-13, MIT, Cambridge, MA, 2012.
Mirabito, C., Haley Jr., P., Lermusiaux, P. F. J., and Leslie, W. G.: A river discharge model for coastal Taiwan during typhoon Morakot, Massachusetts Institute of Technology, Cambridge, 21 pp., 2013.
Nash, D. B.: Effective sediment-transporting discharge from magnitude–frequency analysis, J. Geol., 102, 79–95, 1994.
O'Donnell, J.: The formation and fate of a river plume: a numerical model, J. Phys. Oceanogr., 20, 551–569, 1990.
Orton, G. J. and Reading, H. G.: Variability of deltaic processes in terms of sediment supply, with particular emphasis on grain size, Sedimentology, 40, 475–512, 1993.
Osadchiev, A. A. and Zavialov, P. O.: Lagrangian model for surface-advected river plume, Cont. Shelf. Res., 15, 58, 96–106, 2013.
Ross, O. N. and Sharples, J.: Recipe for 1-D Lagrangian particle tracking models in space-varying diffusivity, Limnol. Oceanogr.-Meth., 2, 289–302, 2004.
Rudnick, D. L., Jan, S., Centurioni, L., Lee, C. M., Lien, R.-C., Wang, J., Lee, D.-K., Tseng, R.-S., Kim, Y. Y., and Chern, C.-S.: Seasonal and mesoscale variability of the Kuroshio near its origin, Oceanography, 24, 52–63, 2011.
Shen, H.-C.: Topography Induced Flow Variations between Taitung-Lutao off Southeast Taiwan, Master's thesis, Institute of Applied Marine Physics and Undersea Technology, National Sun Yat-sen University, Kaoshiung, Taiwan, 138 pp., 2012.
Sholkovitz, E. R.: Flocculation of dissolved organic and inorganic matter during the mixing of river water and seawater, Geochim. Cosmochim. Ac., 40, 831–845, 1976.
Smagorinsky, J.: General circulation experiments with the primitive equation. 1. The basic experiment, Mon. Weather Rev., 91, 99–165, 1963.

NHESSD
3, 5155–5189, 2015

Spagnol, S., Wolanski, E., Deleersnijder, E., Brinkman, R., McAllister, F., Cushman-Roisin, B., and Hanert, E.: An error frequently made in the evaluation of advective transport in two-dimensional Lagrangian models of advection/diffusion in coral reef waters, Mar. Ecol.-Prog. Ser., 235, 299–302, 2002.
Stokes, G. G.: On the effect of the internal friction of fluids on the motion of pendulums, Cambridge Philosophical Transactions, 9, 8–106, 1851.
Syvitski, J. P. M. and Saito, Y.: Morphodynamics of deltas under the influence of humans, Global Planet. Change, 57, 261–282, 2007.
Visser, A. W.: Using random walk models to simulate the vertical distribution of particles in a turbulent water column, Mar. Ecol.-Prog. Ser., 158, 275–281, 1997.
Walsh, J. P. and Nittrouer, C. A.: Understanding fine-grained river-sediment dispersal on continental margins, Mar. Geol., 263, 34–45, 2009.
Warrick, J. A.: Eel River margin source-to-sink sediment budgets: revisited, Mar. Geol., 351, 25–37, 2014.
Warrick, J. A. and Milliman, J. D.: Hyperpycnal sediment discharge from semiarid southern California rivers: implications for coastal sediment budgets, Geology, 31, 781–784, 2003.
Wright, L. D., Friedrichs, C. T., Kim, S. C., and Scully, M. E.: Effects of ambient currents and waves on gravity-driven sediment transport on continental shelves, Mar. Geol., 175, 25–45, 2001.
Wu, L., Liang, J., and Wu, C.-C.: Monsoonal influence on Typhoon Morakot (2009). Part I: Observational analysis, J. Atmos. Sci., 68, 2208–2220, 2011.
Wyrtky, K.: Scientific results of marine investigations of the South China Sea and the Gulf of Thailand, in: NAGA Report, vol. 2, The University of California, Scripps Institution of Oceanography, La Jolla, USA, 1961.
Yu, H. S.: Hyperpycnal discharge of fluvial sediment to the ocean: impact of supertyphoon Herb (1996) on Taiwanese rivers: a discussion, J. Geol., 114, 763–765, 2006.
Yuan, Y., Liu, C., Pan, Z., and Zheng, S.: Circulation east of Taiwan and in the East China Sea and east of Ryukyu Islands during early summer 1985, Acta Oceanol. Sin., 15, 423–435, 1996.
Yuan, Y., Liu, Y., Liu, C., and Su, J.: The Kuroshio east of Taiwan and the currents east of the Ryukyu Islands during October of 1995, Acta Oceanol. Sin., 17, 1–13, 1998.
Zu, T., Gan, J., and Erofeeva, S. Y.: Numerical study of the tide and tidal dynamics in the South China Sea, Deep-Sea Res. Pt. I, 55, 137–154, 2008.

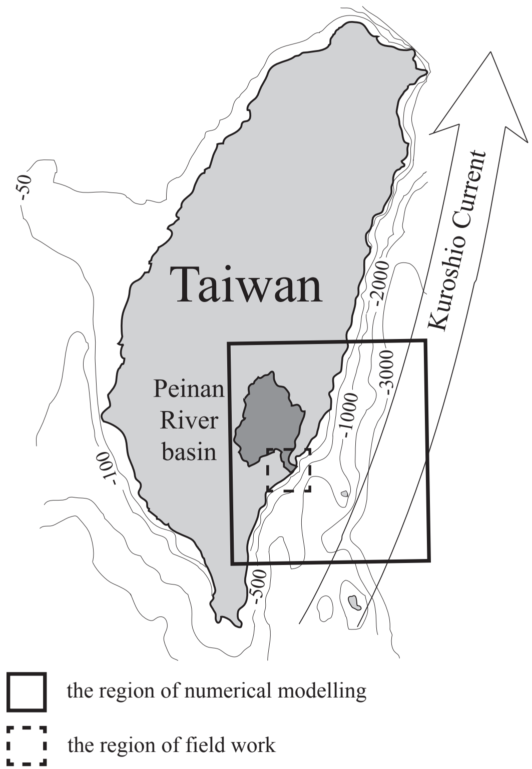

Figure 1. Bathymetry of Taiwan coastal areas and deposition of the study regions at the steep south-eastern shore adjacent to the Peinan River estuary.

NHESSD
3, 5155–5189, 2015

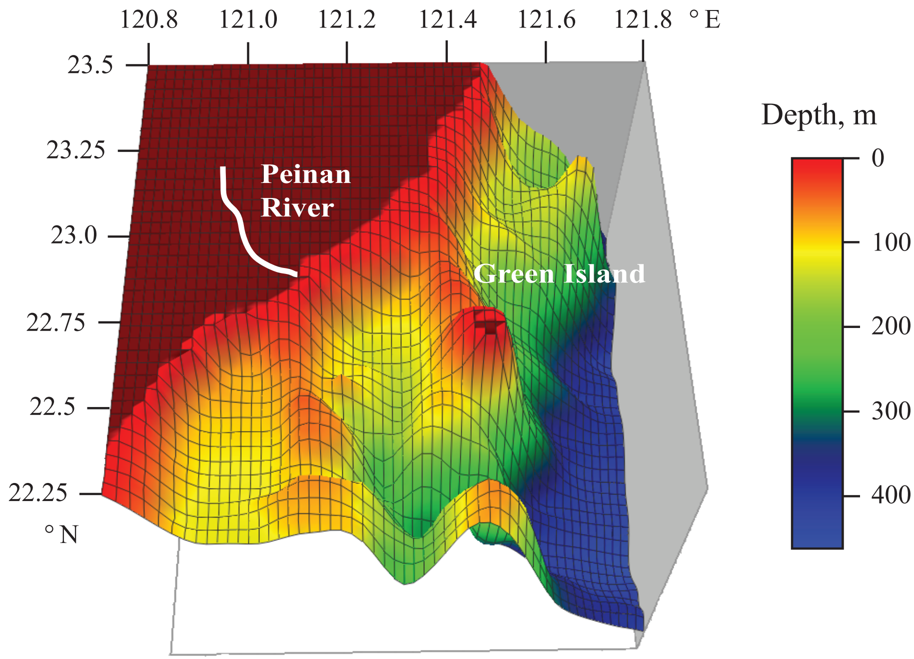

Figure 2. Bathymetry of the region of numerical modelling illustrating deposition of submarine canyons and locations of the Peinan River and the Green Isalnd.

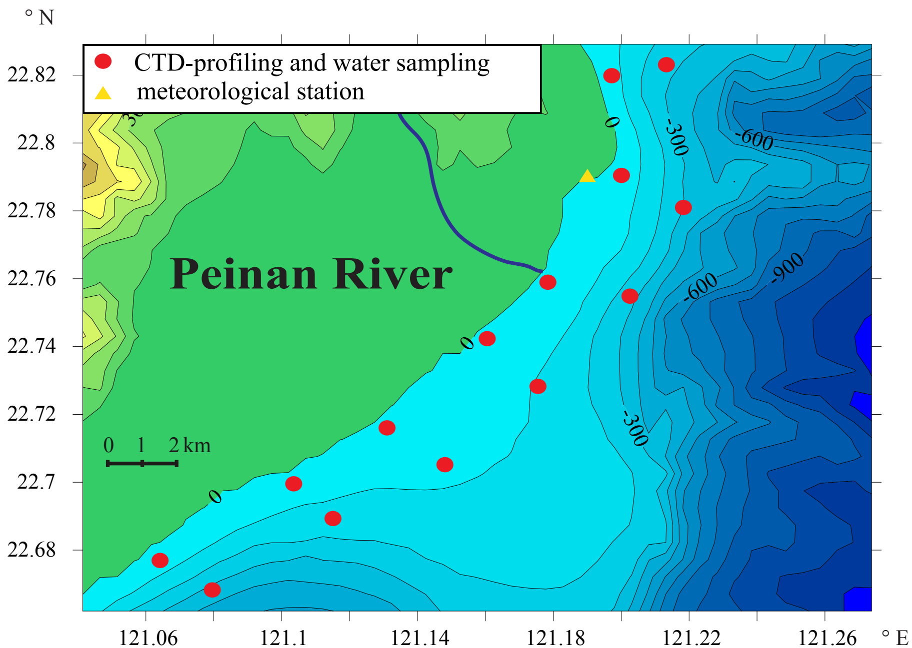

Figure 3. Topography, bathymetry, and location of stations at the region of field work conducted on 15–17 April 2014.

NHESSD
3, 5155–5189, 2015

Transport of river sediments and associated submarine landslides

A. A. Osadchiev et al.

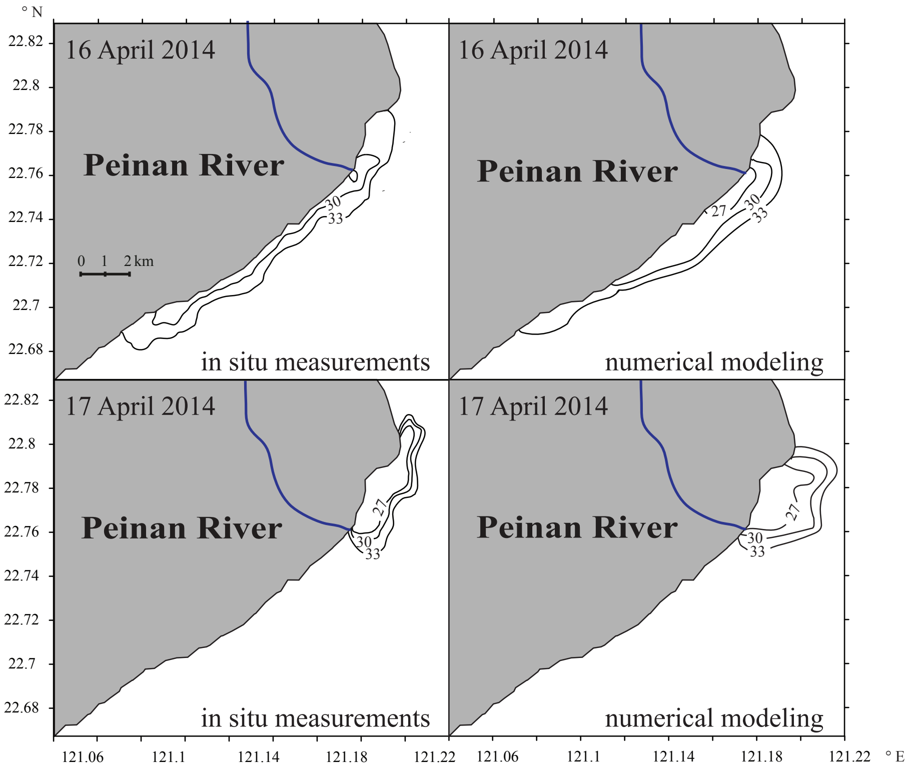

Figure 4. Surface salinity distribution (27, 30, and 33 psu isohalines) illustrating deposition and internal structure of the Peinan river plume obtained from the in situ measurements (left) and simulated by the numerical model (right) on 16 April 2014 (top) and 17 April 2014 (bottom).

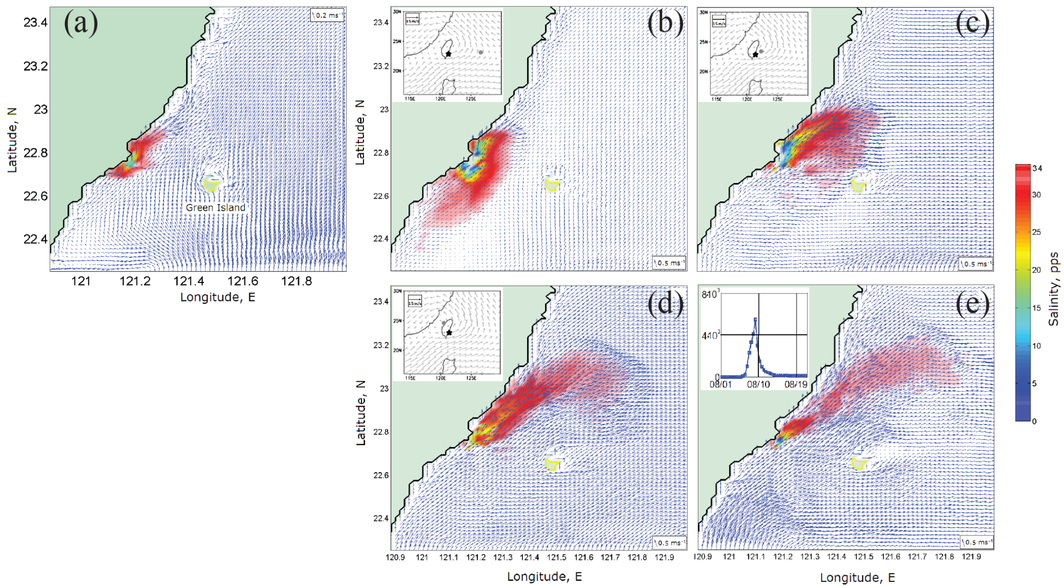

Figure 5. The Peinan River plume under typhoon conditions before **(a)**, on the first **(b)**, the second **(c)**, the third **(d)**, and the fifth **(e)** day of typhoon simulation. Deposition of the center of 700-hPa typhoon (solid dot) and the Peinan River estuary (solid star) are shown in the insets in **(a–c)** (after Wu et al., 2011). The inset in **(e)** shows the increasing of the Peinan River discharge rate ($m^3 s^{-1}$) under typhoon conditions (after Mirabito et al., 2012).

NHESSD
3, 5155–5189, 2015

Transport of river sediments and associated submarine landslides

A. A. Osadchiev et al.

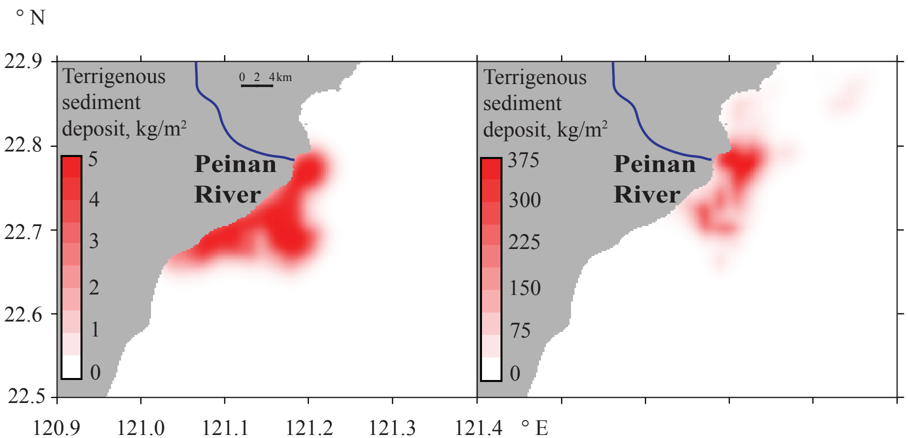

Figure 6. Simulated distribution of fine sediments deposited to the seabed at the study area under moderate (left) and flooding (right) forcing conditions.

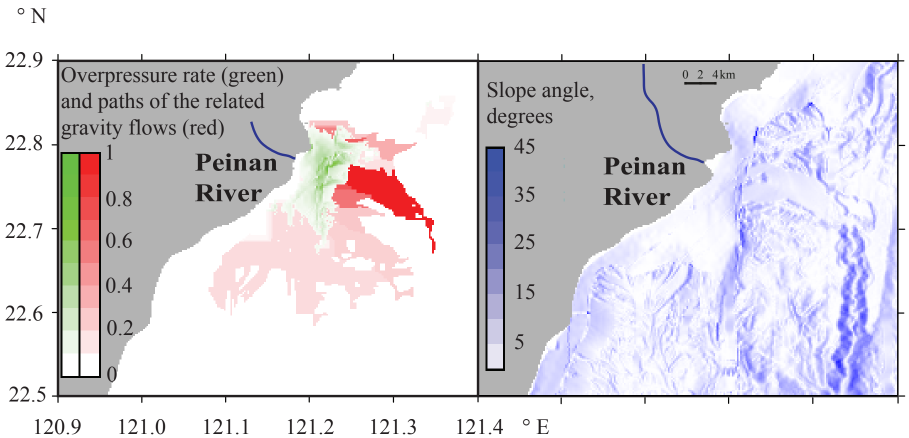

Figure 7. Left column: distribution of the overpressure rate (green) under typhoon discharge conditions and potential paths of the related gravity flows (red). Right column: bottom topography gradient at the region of numerical modelling.

NHESSD
3, 5155–5189, 2015

Transport of river sediments and associated submarine landslides

A. A. Osadchiev et al.